Demonstrating the Affleck-Kennedy-Lieb-Tasaki Spectral Gap on 2D Degree-3 Lattices

Nicholas Pomata[1,*] and Tzu-Chieh Wei[1,2,†]

[1]*C. N. Yang Institute for Theoretical Physics and Department of Physics and Astronomy, State University of New York at Stony Brook, Stony Brook, New York 11794-3840, USA*

[2]*Institute for Advanced Computational Science, State University of New York at Stony Brook, Stony Brook, New York 11794-5250, USA*

(Received 12 November 2019; accepted 9 April 2020; published 28 April 2020)

We report results on solving a long outstanding problem—whether the two-dimensional spin-3/2 antiferromagnetic valence-bond model of Affleck, Kennedy, Lieb, and Tasaki (AKLT) possesses a nonzero gap above its ground state. We exploit a relation between the anticommutator and sum of two projectors and apply it to ground-space projectors on regions of the honeycomb lattice. After analytically reducing the complexity of the resultant problem, we are able to use a standard Lanczos method to establish the existence of a nonzero gap. This approach is also successfully applied to spin-3/2 AKLT models on other degree-3 semiregular tilings, namely, the square-octagon, star, and cross lattices, where the complexity is low enough that exact diagonalization can be used instead. In addition, we close the previously open cases of hybrid AKLT models on the singly decorated honeycomb and singly decorated square lattices.

DOI: 10.1103/PhysRevLett.124.177203

Introduction.—The spectral gap of the Hamiltonian is ubiquitous across disciplines of quantum physics, taking a central position in superconductivity [1], the fractional quantum Hall effect [2], and the Yang-Mills mass gap [3]. Proving its existence in interacting systems is generally hard: the problem can be undecidable even in translation invariant nearest-neighbor spin systems [4]. In one-dimensional spin systems, Haldane conjectured that integer-spin isotropic antiferromagnetic chains could have such a gap, in contrast to half-integer ones [5,6]. This conjecture was substantiated by the construction of a spin-1 chain by Affleck, Kennedy, Lieb, and Tasaki (AKLT) that has exponentially decaying correlations and a provably nonzero gap [7,8]. This chain is now recognized as a paradigmatic example of symmetry-protected topological phases [9–14]. The two-dimensional (2D) models in the original work by AKLT, which likewise display exponentially decaying correlations [7,8,15], can be regarded as examples of 2D Haldane disordered phases [16] whose topological properties are detected by "strange correlators" [17,18]. However, a stable topological phase requires a nonzero gap, and it is much harder to demonstrate the existence of that gap in two or higher dimensions: for example, the gap typically implies exponential decay of ground-state correlation functions [19,20], but not generally vice versa. The existence of such a gap in the original AKLT models has thus evaded proof for more than three decades.

In this Letter, we solve this long-standing question and find a lower bound on the spectral gap in the spin-3/2 AKLT model on the honeycomb lattice, which was also independently established in a recent work by Lemm *et al.* [21] using a different, also numerically assisted, method. We analytically reduce the criterion of the nonzero gap to an eigenvalue problem which we solve with a standard application of the Lanczos method. We also successfully apply this approach to other spin-3/2 AKLT models on the three other 2D Archimedean degree-3 lattices: the square-octagon, star, and cross lattices, for which we can establish the spectral gap with *exact diagonalization*. Beyond these, we demonstrate the existence of a gap in the hybrid AKLT models on the decorated honeycomb and square lattices, where a spin-1 site is added to every edge of the undecorated lattice, which recent studies [22,23] left open.

AKLT wave functions, when expressed in terms of bosonic coherent states, resemble closely the Laughlin wave functions of the fractional quantum Hall effect [24], whose topological properties require by definition a spectral gap which remains largely elusive [25] in their parent Hamiltonians. That bosonic formulation in turn helps to understand magnetic order and disorder in spin systems [26], and enables calculations of certain topological indices [27]. As their "valence-bond" formalism provided us with the first examples of tensor-network states [28,29], AKLT-like systems have also provided insight into the holographic framework [30–32] and enabled studies of various quantum phase transitions [33–35] and of violation of the eigenstate thermalization hypothesis [36]. Moreover, many 2D AKLT states have been shown to serve as resources for universal quantum computation [37–41], which has also motivated a search for AKLT states in solid-state materials [42].

The AKLT construction and tensor networks.—We begin by reviewing the construction of AKLT wave functions [8] and the related tensor-network picture, as shown in Fig. 1. We start with some lattice (more precisely graph) Λ whose vertices host the physical degrees of freedom. On each edge

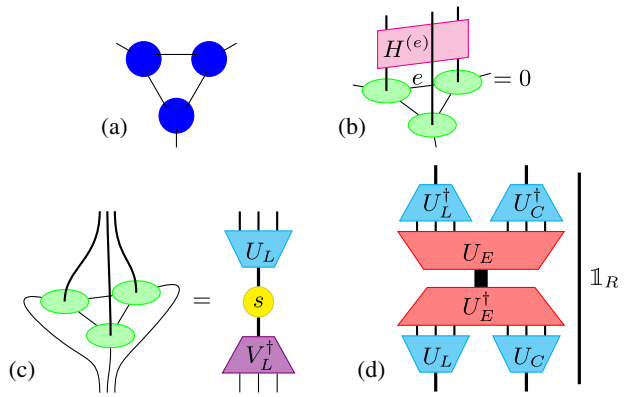

FIG. 1. The AKLT construction and the tensor-network approach for dimensional reduction, using a region in the star lattice [see Fig. 2(a)] as an example. (a) In the standard valence-bond picture, projectors (large circles) are shown acting on spins, which form singlets (line segments) across sites. In the tensor-network picture [shown in (b),(c)], meanwhile, we represent the state as the contraction of tensors (green), virtual and physical indices represented explicitly as light and heavy lines, respectively. (b) The frustration-free condition: the ground state vanishes when any individual Hamiltonian term $H^{(e)}_{\mathrm{AKLT}}$, associated with some edge e, is applied. (c) Using a region L [in this case triangular; see Fig. 2(a)] we define the tensor Ψ_L, as a mapping from virtual to physical spaces; its singular-value decomposition, $\Psi_L = U_L s V_L^\dagger$, defines for us a new space $\mathcal{H}_L$ (in this case isomorphic to the virtual space $\mathcal{H}^L_{\mathrm{virt}}$). (d) Similarly, having determined the isometry U_E (which defines the corresponding projector by $E = U_E U_E^\dagger$) supported on the region $L \cup C$, we project down the physical indices to form $U'_E = (U_L^\dagger \otimes U_C^\dagger) U_E$, reducing E to $E' = U'_E U'^\dagger_E \otimes \mathbb{1}_R$; F' is constructed similarly.

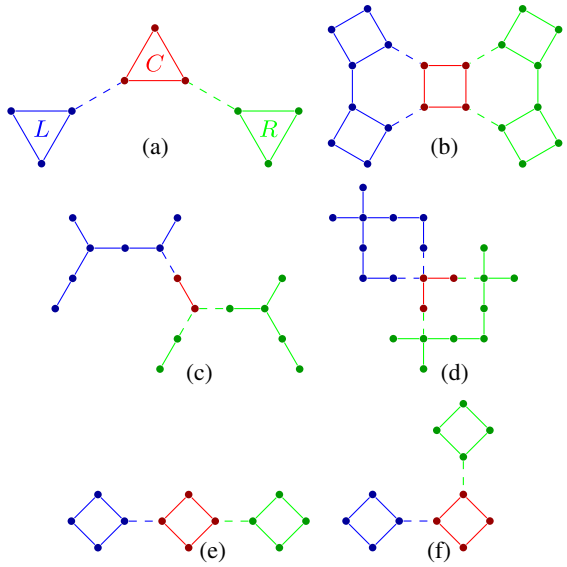

FIG. 2. Overlapping terms in the (a) star, (b) cross, (c) singly decorated honeycomb, (d) singly decorated square lattice, and (e),(f) square-octagon lattices. Shown in red are precisely the regions where they overlap; the two subgraphs Γ_i and Γ_j are the blue and red and red and green regions, respectively: the blue, red, and green regions correspond to the subgraphs L, C, and R, labeled in (a).

we place a spin-singlet state, formed with two virtual spin-1/2 (qubit) degrees of freedom. If a given site has z nearest neighbors in Λ, z total qubits will be associated to that site. Then a spin-$z/2$ projector is applied to these z virtual qubits to produce the physical degree of freedom, as in Fig. 1(a). This valence-bond construction is notably amenable to tensor-network representation: spin singlets are rank-2 tensors and projectors are rank-$(z+1)$ tensors whose z virtual indices are contracted with those singlets. This state has a standard parent Hamiltonian [7,8], constructed explicitly in Sec. F of the Supplemental Material [43], which is defined such that each term $H^{(e)}_{\mathrm{AKLT}}$ associated with an edge e separately annihilates the ground state, as illustrated in Fig. 1(b).

For the purposes of notation and the benefit of readers less familiar with tensor networks, we analyze the above AKLT construction on a subgraph $\Gamma \subset \Lambda$ as follows. The local AKLT wave function Ψ_Γ on Γ is obtained by contracting the tensors corresponding to the vertices and edges of Γ: it will have one physical index for every vertex in Γ and one virtual index for every half-open edge, as illustrated in Fig. 1(c). The physical indices are grouped into a tensor-product Hilbert space $\mathcal{H}^\Gamma_{\mathrm{phys}}$ and the virtual indices are grouped into a tensor-product Hilbert space $\mathcal{H}^\Gamma_{\mathrm{virt}}$. We thus treat Ψ_Γ as a linear map from the dual space $(\mathcal{H}^\Gamma_{\mathrm{virt}})^*$ to $\mathcal{H}^\Gamma_{\mathrm{phys}}$. The AKLT Hamiltonian $H_{\Gamma,\mathrm{AKLT}}$ on Γ is the sum over edges $e \in \Gamma$ of the Hamiltonian terms $H^{(e)}_{\mathrm{AKLT}}$, and from the frustration-free property, $H_{\Gamma,\mathrm{AKLT}}\Psi_\Gamma = 0$.

On this subgraph Γ, we can perform [see Fig. 1(c)] a singular-value decomposition $\Psi_\Gamma = U_\Gamma s V_\Gamma^\dagger$, where the singular-value matrix s is defined to contain only nonzero singular values. This standard tensor-network technique (often known as "projective truncation") allows us to determine the projector Π_Γ onto the ground space in the region (or, subgraph) Γ [e.g., L in Fig. 1(c); equivalently, the "left" triangle in Fig. 2(a)] by $\Pi_\Gamma = U_\Gamma U_\Gamma^\dagger$, as we will use in several places below.

The main question we seek to answer is whether the AKLT Hamiltonian has a spectral gap: that is, if there is a number $\Delta > 0$ such that all excited states of the Hamiltonian have energy greater than Δ for Λ sufficiently large, including in the thermodynamic limit.

The method.—In the following, we describe the basic steps we use to establish the gap in various 2D AKLT models. A simple example, shown in Figs. 1 and 2(a), is the "star" lattice, for which we are able to reduce the size of the matrix needed to diagonalize from $2^{18} \times 2^{18}$ to $2^9 \times 2^9$. These steps are also easily applied to the 1D AKLT chain, as elaborated in Sec. A of the Supplemental Material [43]. In both cases, we provide scripts in Python, for a more

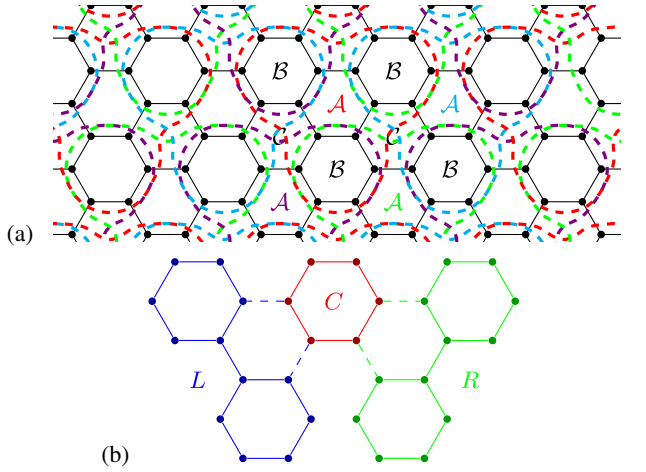

FIG. 3. (a) Enlarged terms of the honeycomb lattice, described below. We identify for several plaquettes which of the three dual sublattices $\mathcal{A}$, $\mathcal{B}$, and $\mathcal{C}$ they belong to. (b) Pairs of adjacent terms, overlapping on hexagonal plaquettes. We apply the "simplifying" isometries U_L, U_R, and U_C to the blue, green, and red regions, respectively.

natural treatment with rigorous checks, and in *Mathematica*, with more illustration and description. We hope that they will show the reader how to bound the gap by assembling the wave function in a region from local tensors, performing singular-value decomposition, and diagonalizing resulting matrices.

(1) Constructing a lower-bounding Hamiltonian: Our first step toward proving the spectral gap is to partition the lattice Λ into overlapping subgraphs Γ_i (which collectively contain all edges of the graph); see, for example, Fig. 3(a). We then define new Hamiltonian terms of the form $\tilde{H}_i = \mathbb{1}_{\Gamma_i,\mathrm{phys}} - \Pi_{\Gamma_i}$, whose ground space on Γ_i is defined to match the original AKLT state; Π_{Γ_i}, which projects onto that ground space, is obtained as explained above and illustrated in Fig. 1(c). In order to compare this to the original AKLT Hamiltonian, we must find a $\gamma_0 > 0$ such that

$$H_{\Gamma_i} \equiv \sum_{e\in\Gamma_i} \frac{1}{n_e} H^{(e)}_{\mathrm{AKLT}} \geq \gamma_0 \tilde{H}_i, \tag{1}$$

where n_e is the number of i for which $e \in \Gamma_i$, and γ_0 will be the spectral gap of the locally defined H_{Γ_i}. Thus, we can lower bound the original AKLT Hamiltonian by the new Hamiltonian $\tilde{H}$,

$$H_{\mathrm{AKLT}} = \sum_{e\in\Lambda} H^{(e)}_{\mathrm{AKLT}} = \sum_i \sum_{e\in\Gamma_i} \frac{1}{n_e} H^{(e)}_{\mathrm{AKLT}} \geq \gamma_0 \sum_i \tilde{H}_i. \tag{2}$$

The Hamiltonian $\tilde{H} \equiv \sum_i \tilde{H}_i$ enables us to lower bound the gap of H_{AKLT}: if, for some $\tilde{\gamma} > 0$,

$$\tilde{H}^2 \geq \tilde{\gamma}\, \tilde{H}, \tag{3}$$

then $\tilde{H}$ has a gap of at least $\tilde{\gamma}$ and thus H_{AKLT} has a gap of at least $\gamma_0\tilde{\gamma}$.

(2) Reducing the gap criterion to an eigenvalue problem: As the $\tilde{H}_i$'s are projectors, we follow a standard practice [22,44] to write

$$\tilde{H}^2 = \sum_i \tilde{H}_i + \sum_{i\neq j} \tilde{H}_i \tilde{H}_j, \tag{4}$$

$$\geq \tilde{H} + \sum_{\langle i,j\rangle} \{\tilde{H}_i, \tilde{H}_j\} \geq (1 - \eta\tilde{z})\tilde{H}, \tag{5}$$

where the sum in (5) is over "nearest neighbors" $\langle i, j\rangle$ [see Figs. 2 and 3(b)] such that the corresponding regions have nonzero overlap, i.e., $\Gamma_i \cap \Gamma_j \neq \varnothing$, and where $\tilde{z}$ is the (maximal) number of nearest neighbors per term and η is defined by (5), i.e., it is the least positive number such that [44]

$$\{\tilde{H}_i, \tilde{H}_j\} \equiv \tilde{H}_i\tilde{H}_j + \tilde{H}_j\tilde{H}_i \geq -\eta(\tilde{H}_i + \tilde{H}_j). \tag{6}$$

Our method for establishing the spectral gap centers around partitioning Λ into sufficiently large regions Γ_i that $\tilde{\gamma} = 1 - \eta\tilde{z} > 0$.

It is known that (see Lemma 6.3a of [44]) if Eq. (6) holds, then it also holds when we replace $\tilde{H}_i$ and $\tilde{H}_j$ by their complements $E \equiv \Pi_{\Gamma_i} = \mathbb{1}_i - \tilde{H}_i$ and $F \equiv \Pi_{\Gamma_j} = \mathbb{1}_j - \tilde{H}_j$, respectively. In [23], we have proven the key fact that

> *For η optimal in (6), $1 \pm \eta$ are the greatest and least, respectively, noninteger eigenvalues of $E + F$.*

This allows us to extract η from the spectrum of $E + F$ (or even just the greatest eigenvalues). However, this operator will often be prohibitively large to analyze directly via exact diagonalization; for example, in the case of the honeycomb lattice [illustrated in Fig. 3(b)], the full matrix has size $2^{60} \times 2^{60}$. Fortunately, we can take advantage of the tensor-network construction of AKLT models to reduce the complexity of the problem. Given two overlapping regions Γ_i and Γ_j, we have shown in [23] that

> *The local definition of the projector $\Pi_L = U_L U_L^\dagger$ acting on the "left" region $L \equiv \Gamma_i \backslash \Gamma_j$ means that the spectra of $E + F$ and the "reduced" operator $U_L^\dagger(E + F)U_L$ are identical (at least, for all noninteger values). This is also true for Π_R defined on the "right" region $R \equiv \Gamma_j \backslash \Gamma_i$ and for Π_C defined on the "center" region $C \equiv \Gamma_i \cap \Gamma_j$.*

We illustrate the regions L, C, and R in Figs. 2(a) and 3(b).

We apply these three simplifying projectors (or more precisely, isometries) to E and F, as in Fig. 1(d), to produce the reduced operators E' and F'.

(3) Diagonalization: Here we summarize the different diagonalization methods we use to extract the number η

TABLE I. For each configuration considered, the extracted value of η; the number of intersections $\tilde{z}$ of the type that this particular η applies to, the total dimension $D_{\text{tot}} \equiv \dim(\mathcal{H}_L \otimes \mathcal{H}_C \otimes \mathcal{H}_R)$ of the space on which the operators $E' + F'$ act, the bound γ_0 that relates the modified Hamiltonian to the original, and the bound Δ_{lower} on the gap. Results are given to four digits of precision; for ten digits, see Table III of the Supplemental Material [43].

	Method	η	$\tilde{z}$	D_{tot}	γ_0	Δ_{lower}
Square-octagon	I	0.1062	2	2^{12}		
	I	0.1590	4		0.05453	0.008281
Star	I	0.1111	4	2^{9}	0.1417	0.07876
Cross	I	0.1998	3	2^{16}	0.08232	0.03299
Honeycomb	IIb	0.1446	6	2^{26}	0.04107×0.7784	0.004250
Decorated lattices, $n = 1$						
Honeycomb	I	0.1531	4	$2^{7}3^{4}$	0.2051	0.02743
Square	IIa	0.2204	4	$2^{12}3^{4}$	0.1223	0.01450

from the tensors we have constructed, depending on computational memory requirements, listed below in increasing order of complexity (the complete details can be found in Sec. E of the Supplemental Material [43]). (i) When we can represent the operator $E' + F'$ densely in memory, we exactly diagonalize it. (iia) If not, we apply iterative, Lanczos diagonalization: we subtract Π'_Y, defined to project onto the two-eigenspace of $E' + F'$, from $E' + F'$, so as to make $1 + \eta$ the largest eigenvalue. (iib) Sometimes Π'_Y is also too large to construct. In this case, we linearly combine the mutually commuting operators (a) $E' + F'$; (b) $E'F' + F'E'$; and (c) ρ'_Y, an unnormalized operator whose support is exactly the 2-eigenspace of $E' + F'$, so as to maximize the eigenvalue corresponding to $1 + \eta$ in $E' + F'$, and extract η from Lanczos diagonalization of that.

Note that these methods are designed to analyze the spectrum of the same operator $E + F$ via standard LAPACK and ARPACK implementations of exact and Lanczos diagonalization and are all highly precise, ensuring more than ten digits of accuracy.

Results.—A summary of values of the key parameter η, relevant dimensions, and other information is shown in Table I. Here we review how we have repartitioned these lattices, an essential part of our technique. We illustrate the case of the honeycomb lattice in detail in Fig. 3 and the other cases more briefly in Fig. 2 (for more detail, see the Supplemental Material [43]).

(1) The honeycomb lattice: We first tripartition the dual lattice; call the resultant sets of plaquettes $\mathcal{A}$, $\mathcal{B}$, and $\mathcal{C}$. Then, as shown in Fig. 3, we assign for each plaquette $p \in \mathcal{A}$ a subgraph Γ_p consisting of p and the three neighboring plaquettes belonging to $\mathcal{B}$. Then the overlapping subgraphs consist of nearest neighbors of the triangular lattice whose vertices are the elements of $\mathcal{A}$; in particular, each term overlaps with six other terms, so we must find $\eta < \frac{1}{6}$. As shown in Fig. 3(b), the overlapping subgraph C is a hexagon, whereas the outside subgraphs L and R consist of nonintersecting hexagonal plaquettes joined by a single edge. These allow us to reduce the dimension of the space on which $E + F$ acts (30 spin-3/2 sites in total) from $4^{30} = 2^{60}$ to the dimension of the space that $E' + F'$ acts on

$$D_{\text{tot}} \equiv \dim(\mathcal{H}_L \otimes \mathcal{H}_C \otimes \mathcal{H}_R) = 2^{26}. \tag{7}$$

We then determine, using the Lanczos diagonalization algorithm as implemented in standard ARPACK libraries to realize method IIb, that $\eta = 0.1445124916 < \frac{1}{6}$, and thus the model is gapped. As described in more detail in Sec. D of the Supplemental Material [43], we use a two-step method to establish a lower bound on the gap,

$$\Delta_{\text{lower}} = \gamma^{[2p]}\gamma^{[4p]}(1 - 6\eta) = 0.004250539442, \tag{8}$$

where $\gamma^{[2p]} = 0.04107930111$ and $\gamma^{[4p]} = 0.7784203312$.

2. The [4.8.8] square-octagon lattice: The new terms we consider correspond to an edge dividing a given pair of octogonal plaquettes and the two square plaquettes it connects, as shown in Figs. 2(e) and 2(f). Here each such subgraph overlaps with six others; uniquely among the lattices we are considering, the overlaps between these subgraphs have two different forms. We categorize these pairs (Π_{Γ_i} and Π_{Γ_j}) using the edges connecting the square plaquettes, which can be either collinear [Fig. 2(e), say $i \| j$] or perpendicular [Fig. 2(f), say $i \perp j$]. We must then modify (6) and (5) to read

$$\begin{aligned} \{\tilde{H}_i, \tilde{H}_j\} &\geq -\eta_{\|}(\tilde{H}_i + \tilde{H}_j), \quad i \| j \\ &\geq -\eta_{\perp}(\tilde{H}_i + \tilde{H}_j), \quad i \perp j, \end{aligned} \tag{9}$$

$$\tilde{H}^2 \geq (1 - 2\eta_{\|} - 4\eta_{\perp})\tilde{H}. \tag{10}$$

In particular, for the gap to exist, we need $4\eta_{\perp} + 2\eta_{\|} < 1$. This is satisfied by the values we extract of $\eta_{\|} = 0.1061446858$ and $\eta_{\perp} = 0.1589663310$, via exact diagonalization (method I).

3. The [3.12.12] star lattice: Here we select subgraphs consisting of the edge dividing a pair of dodecagonal plaquettes and the two triangular plaquettes it connects; see Fig. 2(a). Now each such subgraph overlaps with four others, and we find that $\eta = 0.1110430220 < \frac{1}{4}$.

4. The [4.6.12] "cross" lattice: We select subgraphs corresponding to a hexagonal plaquette plus the three adjoining square plaquettes; see Fig. 2(b). Each such subgraph overlaps with three others, one for each square plaquette. We find that $\eta = 0.1997384500 < \frac{1}{3}$.

5. The decorated honeycomb lattice: We now consider the honeycomb lattice with *one decoration* per edge. The subgraphs we choose are the "H" shapes shown in Fig. 2(c), consisting of a "horizontal" edge $v - w$ together with the decorations "above" v and w and the full edge "below" each of v and w. Then each subgraph overlaps with four others, at each of the four segments (half-edges) at its boundaries. We find that $\eta = 0.1530329085 < \frac{1}{4}$.

6. The decorated square lattice: In this sixth model, we consider the square lattice with one decoration per edge. We first bipartition the dual lattice into sublattices $\mathcal{A}$ and $\mathcal{B}$ and then further bipartition $\mathcal{A}$ into $\mathcal{A}_1$ and $\mathcal{A}_2$. For $p \in \mathcal{A}_1$, we add the decorations adjoining the lower-right and upper-left corners [blue in Fig. 2(d)]; for $p \in \mathcal{A}_2$ we add those on the lower-left and upper-right corners [green in Fig. 2(d)]. These subgraphs then have three-vertex intersections with four other subgraphs, at each corner of the original plaquette. We find that $\eta = 0.2203543174 < \frac{1}{4}$, establishing a nonzero gap.

These last two results, in combination with [22,23], prove that the AKLT Hamiltonians on the decorated square and honeycomb lattices are gapped for all $n > 0$.

Concluding remarks.—We have proven the existence of a nonzero spectral gap in the original 2D AKLT model on the honeycomb lattice, a problem which has been open for more than three decades [7,8]. We have also demonstrated the versatility of our method by bounding the gap of five other Hamiltonians. The spectral gap in spin-2 AKLT models on the square lattice and other degree-4 lattices should be possible to attack using our method. If the relevant vector spaces are too large to diagonalize exactly or iteratively, then one may need to further refine these methods. Beyond AKLT models, our approach applies in general to models constructed using the projected-entangled-pair-state formalism [45,46].

This work was partially supported by the National Science Foundation under Grant No. PHY 1915165.

*nicholas.pomata@stonybrook.edu
†tzu-chieh.wei@stonybrook.edu

[1] J. Bardeen, L. N. Cooper, and J. R. Schrieffer, Theory of superconductivity, Phys. Rev. **108**, 1175 (1957).
[2] S. M. Girvin, The quantum Hall effect: Novel excitations and broken symmetries, in *Aspects Topologiques de la Physique en Basse Dimension. Topological Aspects of Low Dimensional Systems* (Springer, Grenoble, 1999), pp. 53–175.
[3] A. Jaffe and E. Witten, Quantum Yang-Mills theory, in *The Millennium Prize Problems*, edited by J. A. Carlson, A. Jaffe, and A. Wiles (Clay Mathematics Institute, AMS, Cambridge, MA, 2006), pp. 129–152.
[4] T. S. Cubitt, D. Perez-Garcia, and M. M. Wolf, Undecidability of the spectral gap, Nature (London) **528**, 207 (2015).
[5] F. D. M. Haldane, Nonlinear field theory of large-spin Heisenberg Antiferromagnets: Semiclassically Quantized Solitons of the One-Dimensional Easy-Axis Néel State, Phys. Rev. Lett. **50**, 1153 (1983).
[6] I. Affleck, Quantum spin chains and the Haldane gap, J. Phys. Condens. Matter **1**, 3047 (1989).
[7] I. Affleck, T. Kennedy, E. H. Lieb, and H. Tasaki, Rigorous Results on Valence-Bond Ground States in Antiferromagnets, Phys. Rev. Lett. **59**, 799 (1987).
[8] I. Affleck, T. Kennedy, E. H. Lieb, and H. Tasaki, Valence bond ground states in isotropic quantum antiferromagnets, Commun. Math. Phys. **115**, 477 (1988).
[9] Z.-C. Gu and X.-G. Wen, Tensor-entanglement-filtering renormalization approach and symmetry-protected topological order, Phys. Rev. B **80**, 155131 (2009).
[10] F. Pollmann, E. Berg, A. M. Turner, and M. Oshikawa, Symmetry protection of topological phases in one-dimensional quantum spin systems, Phys. Rev. B **85**, 075125 (2012).
[11] X. Chen, Z.-C. Gu, Z.-X. Liu, and X.-G. Wen, Symmetry-protected topological orders in interacting bosonic systems, Science **338**, 1604 (2012).
[12] X. Chen, Y.-M. Lu, and A. Vishwanath, Symmetry-protected topological phases from decorated domain walls, Nat. Commun. **5**, 3507 (2014).
[13] T. Kariyado, T. Morimoto, and Y. Hatsugai, Z_N Berry Phases in Symmetry Protected Topological Phases, Phys. Rev. Lett. **120**, 247202 (2018).
[14] H. Tasaki, Topological Phase Transition and z_2 Index for $s = 1$ Quantum Spin Chains, Phys. Rev. Lett. **121**, 140604 (2018).
[15] T. Kennedy, E. H. Lieb, and H. Tasaki, A two-dimensional isotropic quantum antiferromagnet with unique disordered ground state, J. Stat. Phys. **53**, 383 (1988).
[16] F. D. M. Haldane, O(3) Nonlinear σ Model and the Topological Distinction Between Integer- and Half-Integer-Spin Antiferromagnets in Two Dimensions, Phys. Rev. Lett. **61**, 1029 (1988).
[17] Y.-Z. You, Z. Bi, A. Rasmussen, K. Slagle, and C. Xu, Wave Function and Strange Correlator of Short-Range Entangled States, Phys. Rev. Lett. **112**, 247202 (2014).
[18] K. Wierschem and K. S. D. Beach, Detection of symmetry-protected topological order in AKLT states by exact evaluation of the strange correlator, Phys. Rev. B **93**, 245141 (2016).
[19] B. Nachtergaele and R. Sims, Lieb-Robinson bounds and the exponential clustering theorem, Commun. Math. Phys. **265**, 119 (2006).
[20] M. B. Hastings and T. Koma, Spectral gap and exponential decay of correlations, Commun. Math. Phys. **265**, 781 (2006).

[21] M. Lemm, A. W. Sandvik, and L. Wang, preceding Letter, Existence of a Spectral Gap in the Affleck-Kennedy-Lieb-Tasaki Model on the Hexagonal Lattice, Phys. Rev. Lett. **124**, 177204 (2020).

[22] H. Abdul-Rahman, M. Lemm, A. Lucia, B. Nachtergaele, and A. Young, A class of two-dimensional AKLT models with a gap, in *Contemporary Mathematics*, Vol. 741, edited by H. Abdul-Rahman, R. Sims, and A. Young (American Mathematical Society, Providence, RI, 2020), pp. 1–21.

[23] N. Pomata and T.-C. Wei, AKLT models on decorated square lattices are gapped, Phys. Rev. B **100**, 094429 (2019).

[24] D. P. Arovas, A. Auerbach, and F. D. M. Haldane, Extended Heisenberg Models of Antiferromagnetism: Analogies to the Fractional Quantum Hall Effect, Phys. Rev. Lett. **60**, 531 (1988).

[25] S. M. Girvin, The quantum Hall effect: Novel excitations and broken symmetries, in *Topological Aspects of Low Dimensional Systems*, edited by A. Comtet, T. Jolicoeur, S. Ouvry, and F. David (Springer, Grenoble, 1999), pp. 53–175.

[26] S. A. Parameswaran, S. L. Sondhi, and D. P. Arovas, Order and disorder in AKLT antiferromagnets in three dimensions, Phys. Rev. B **79**, 024408 (2009).

[27] Z. Huang, W. Zhu, D. P. Arovas, J.-X. Zhu, and A. V. Balatsky, Invariance of Topological Indices Under Hilbert Space Truncation, Phys. Rev. Lett. **120**, 016403 (2018).

[28] F. Verstraete, V. Murg, and J. I. Cirac, Matrix product states, projected entangled pair states, and variational renormalization group methods for quantum spin systems, Adv. Phys. **57**, 143 (2008).

[29] R. Orús, Tensor networks for complex quantum systems, Nat. Rev. Phys. **1**, 538 (2019).

[30] S. Yang, L. Lehman, D. Poilblanc, K. Van Acoleyen, F. Verstraete, J. I. Cirac, and N. Schuch, Edge Theories in Projected Entangled Pair State Models, Phys. Rev. Lett. **112**, 036402 (2014).

[31] J. I. Cirac, D. Poilblanc, N. Schuch, and F. Verstraete, Entanglement spectrum and boundary theories with projected entangled-pair states, Phys. Rev. B **83**, 245134 (2011).

[32] J. Lou, S. Tanaka, H. Katsura, and N. Kawashima, Entanglement spectra of the two-dimensional Affleck-Kennedy-Lieb-Tasaki model: Correspondence between the valence-bond-solid state and conformal field theory, Phys. Rev. B **84**, 245128 (2011).

[33] H. Niggemann, A. Klümper, and J. Zittartz, Quantum phase transition in spin-3/2 systems on the hexagonal lattice—optimum ground state approach, Z. Phys. B **104**, 103 (1997).

[34] N. Pomata, C.-Yu Huang, and T.-C. Wei, Phase transitions of a two-dimensional deformed Affleck-Kennedy-Lieb-Tasaki model, Phys. Rev. B **98**, 014432 (2018).

[35] L. Zhang and F. Wang, Unconventional Surface Critical Behavior Induced by a Quantum Phase Transition from the Two-Dimensional Affleck-Kennedy-Lieb-Tasaki Phase to a Néel-Ordered Phase, Phys. Rev. Lett. **118**, 087201 (2017).

[36] S. Moudgalya, N. Regnault, and B. A. Bernevig, Entanglement of exact excited states of Affleck-Kennedy-Lieb-Tasaki models: Exact results, many-body scars, and violation of the strong eigenstate thermalization hypothesis, Phys. Rev. B **98**, 235156 (2018).

[37] T.-C. Wei, I. Affleck, and R. Raussendorf, Affleck-Kennedy-Lieb-Tasaki State on a Honeycomb Lattice is a Universal Quantum Computational Resource, Phys. Rev. Lett. **106**, 070501 (2011).

[38] A. Miyake, Quantum computational capability of a 2D valence bond solid phase, Ann. Phys. (Amsterdam) **326**, 1656 (2011).

[39] T.-C. Wei, Quantum computational universality of Affleck-Kennedy-Lieb-Tasaki states beyond the honeycomb lattice, Phys. Rev. A **88**, 062307 (2013).

[40] T.-C. Wei, P. Haghnegahdar, and R. Raussendorf, Hybrid valence-bond states for universal quantum computation, Phys. Rev. A **90**, 042333 (2014).

[41] T.-C. Wei and R. Raussendorf, Universal measurement-based quantum computation with spin-2 Affleck-Kennedy-Lieb-Tasaki states, Phys. Rev. A **92**, 012310 (2015).

[42] M. Koch-Janusz, D. I. Khomskii, and E.n Sela, Affleck-Kennedy-Lieb-Tasaki State on a Honeycomb Lattice from t_{2g} Orbitals, Phys. Rev. Lett. **114**, 247204 (2015).

[43] See Supplemental Material at http://link.aps.org/supplemental/10.1103/PhysRevLett.124.177203 for details of our numerical algorithm; the rigorous analytical results on which it relies; simple examples of our algorithm in use & implementations of those examples in Python and *Mathematica*; and a detailed description of the steps for bounding the modified Hamiltonian relative to the original Hamiltonian.

[44] M. Fannes, B. Nachtergaele, and R. F. Werner, Finitely correlated states on quantum spin chains, Commun. Math. Phys. **144**, 443 (1992).

[45] D. Perez-Garcia, F. Verstraete, M. M. Wolf, and J. I. Cirac, PEPS as unique ground states of local Hamiltonians, Quantum Inf. Comput. **8**, 650 (2008).

[46] J. I. Cirac, J. Garre-Rubio, and D. Pérez-García, Mathematical open problems in projected entangled pair states, Rev. Mat. Complutense **32**, 579 (2019).